The Disaster Resilience Value of Rooftop Solar in Residential Communities

Siddharth Patel[*], Luis Ceferino[*], Chenying Liu[*], Anne Kiremidjian[*], and Ram Rajagopal[*†]

[*]Department of Civil and Environmental Engineering, Stanford University
[†]Department of Electrical Engineering (by Courtesy), Stanford University

Abstract

Distributed energy resources can enhance community resilience to power outages in the aftermath of natural disasters. We develop a method to quantify the resilience value that rooftop solar can provide to residential neighborhoods. As a case study, the method is applied to single family homes in San Carlos subjected to an earthquake based on the 1906 San Francisco event. We characterize the impact on resilience of increasing adoption of rooftop solar and of grouping homes into resilience clusters for energy sharing. Policy intervention can ensure more geographically uniform adoption of solar and therefore more even resilience. We evaluate the effect and cost of such an intervention.

1 Introduction

Community resilience is receiving increased attention as climate change threatens more frequent catastrophic weather events and as improved technology enhances the ability of people to respond [1–4]. Hurricanes Irma and Maria severely damaged the electric grids in Florida and Puerto Rico, respectively, leading to widespread and prolonged power outages [5, 6]. Earthquakes also cause significant damage to power systems [7–9]. For example, the medium-size Mw 6.0 Napa earthquake left 70,000 residents completely without power in 2014 [10]. Distributed energy resources, such as rooftop solar and storage, are gaining commercial traction and have the potential to mitigate the impact of catastrophic events by generating and managing energy locally when the centralized grid is out of service [11–15].

Public entities are studying the combined sustainability and resilience benefits of microgrids, which are a group of interconnected loads (i.e., power demands) and distributed energy resources (i.e., generation and storage) that can connect and disconnect to the main grid [16–19]. A microgrid can act as an independent entity and sustain itself for an extended period of time. Evidence has shown that microgrids can increase the disaster resilience of power systems. The Roppongi Hills and the Sendai microgrids functioned as secure power islands following the 2011 Tohoku earthquake and tsunami in Japan [20]. However, there are key microgrid policy questions that need to be addressed to guide their deployment in communities in a way that maximizes the power resilience benefit. For example, what types of distributed energy resources are more effective in microgrids? How should they be sized? And where should they be located? Also in question is whether significant policy interventions will be required to achieve resilience goals. Modeling and quantifying how distributed

energy resources can improve resilience is a necessary prerequisite to answering these questions. In its roadmap for the commercialization of microgrids, the California Energy Commission identified the development and validation of metrics of resilience benefit as a key next step. Our study addresses just that need.

We characterize how the adoption of rooftop solar can improve residential community resilience in terms of electrical energy in the aftermath of a Mw 8.0 earthquake scenario representing the 1906 San Francisco event. Specifically, we study how likely it is that rooftop solar systems can supply enough energy in a day to meet the needs of a group of homes, assuming they reduce their energy consumption by some fraction in the aftermath of the earthquake. We use energy consumption and building construction data for single family homes in the city of San Carlos, California. We do not consider the problem of the mismatch in timing between solar generation and energy consumption, nor do we address how to physically share electrical energy within a group of homes. These challenges could be addressed by energy storage devices, the use of electric vehicles as mobile storage units, and reconfigurable microgrids built into the distribution grid infrastructure. We provide a first-cut analysis of whether the daily energy balance will work out, which is a simpler and more fundamental question.

We focus on net-zero sized solar systems, which renewably generate 100% of a home's electrical energy needs over a certain time span. Net-zero sizing is in line with explicit policy goals in California [21, 22]. We quantify the effect of increasing adoption of rooftop solar on power resilience. We also quantify the improvement in resilience gained by grouping homes together into clusters that share energy, and we identify a threshold for cluster size that obtains most of the benefit. Finally, we compare the resilience provided by two different adoption patterns - one in which households choose to adopt rooftop solar based on their own economic benefit, and another in which a policy intervention ensures more diffuse adoption of solar. We estimate the cost of such an intervention.

2 Model and Method

2.1 Defining risk

Consider a community of N single family homes $H = \{H_1, \ldots, H_N\}$. The electrical energy used by home H_i is l_i, with $l_{i,d}$ being the usage on day d. Let A be an adoption scenario that defines which homes have a rooftop solar panel, sized to be net-zero, and which do not. For the homes that have adopted, the indicator variable $q_i(A) = 1$; otherwise, $q_i(A) = 0$. If home H_i has a solar panel, the panel generates energy $e_{i,d}$ on day d.

Let $V = \{V_1, \ldots, V_M\}$ be a partition of H; each home belongs to exactly one element of V. We call the elements of V resilience clusters. A resilience cluster is a group of homes that cooperate to share energy in case of an outage of the main grid.

Now suppose a catastrophe C occurs, which causes a power outage with a span of $s(C)$ days. The catastrophe also destroys some of the homes. Let $x_i(C) = 1$ if home H_i is uninhabitable after event C, and 0 otherwise. We assumed that, in the immediate aftermath of the earthquake, all homes will reduce their electricity consumption to a fraction f of the pre-earthquake consumption.

Consider a sequence of days T as the time span of analysis, which could be a season or an entire year. Let $S(C, T)$ be the set of all spans of length $s(C)$ in T. For example, if T is a 90 day season, and if $s(C)$ is 3, then $S(C, T)$ is the set of all 88 spans of 3 consecutive days in T. Let $\tilde{s}$ be chosen uniformly at random from $S(C, T)$. We define the risk for cluster V_j over period T for event C as

the probability that if event C happens, the homes in the cluster will be unable to generate enough energy to meet their reduced load for at least one day in the randomly chosen span $\tilde{s}$. Formally:

$$R(V_j, T, C) = P\Big[\bigcup_{d\in\tilde{s}}\Big(\sum_{H_i\in V_j} fl_{i,d} > \sum_{H_i\in V_j}\big(1 - x_i(c)\big)e_{i,d}\Big)\Big] \tag{1}$$

We include the loads of homes rendered uninhabitable by the event under the following framework. The electrical energy usage of a home can be conceptually divided into baseline usage by always-on devices (e.g., a refrigerator) versus active usage initiated by occupants (e.g., a toaster). If a home is uninhabitable, its occupants will move in with a neighbor in their resilience cluster, bringing their active usage with them. Furthermore, even though the uninhabitable home may be structurally unsound, its electrical wiring may still be in place and some of its baseline usage may continue. By contrast, we assume that uninhabitable homes with solar panels cannot generate energy, under the assumption that the panels are destroyed or that they enter a fault state that cannot be cleared without human intervention.[1]

2.2 Empirical estimation

The daily load and solar energy generation for a household are random variables. There is also uncertainty in which homes would be uninhabitable as a result of earthquake damage. We use a realization of daily load and daily solar generation for each household, as well as multiple Monte Carlo realizations of building damage due to the earthquake shaking, in order to generate an empirical estimate of the risk.

Let $\tilde{l}_{i,d}$ and $\tilde{e}_{i,d}$ be the realized load and solar generation. Let $\tilde{C}$ be a set of equally likely realizations of a given earthquake scenario C. Each element $\tilde{c}$ of $\tilde{C}$ is a particular realization, associated with a span of $s(\tilde{c})$ as well as a set of homes rendered uninhabitable for which $x_i(\tilde{c}) = 1$.

The empirically estimated risk is an average taken across all earthquake realizations and spans:

$$\hat{R}(V_j, T, C) = \frac{\sum_{\tilde{c}\in\tilde{C}}\ \sum_{\tilde{s}\in S(\tilde{c},T)} \mathbb{1}\Big\{\bigcup_{d\in\tilde{s}}\Big(\sum_{H_i\in V_j} f\tilde{l}_{i,d} > \sum_{H_i\in V_j}\big(1 - x_i(\tilde{c})\big)\tilde{e}_{i,d}\Big)\Big\}}{\sum_{\tilde{c}\in\tilde{C}} |S(\tilde{c}, T)|}, \tag{2}$$

where $\mathbb{1}\{\cdot\}$ is the indicator function, which evaluates to 1 if its argument is true and 0 if it is false. Note that $|S(\tilde{c}, T)| = |T| - (s(\tilde{c}) - 1)$.

2.3 Cluster size and risk

Here we present a simple, stylized model that demonstrates that increasing cluster size does not necessarily reduce risk. Consider a single time period with homogeneous households. Each household has an independent and identically distributed load $l_i \sim \mathcal{N}(\mu_L, \sigma_L^2)$, with $\mu_L > 0$. All households in the cluster are nearby each other, so they experience the same solar irradiance $I \sim \mathcal{N}(\mu_S, \sigma_S^2)$, with $\mu_S > 0$, which is independent of the household loads. The solar panel for a household scales with its

[1] There is some evidence that rooftop solar panels can survive natural disasters [23], but returning them to an operational state is a separate matter. For example, residents may be unable or unwilling to enter a partially destroyed home in order to reset inverters or otherwise get their rooftop panels into an operational state.

mean consumption, as in net-zero sizing, so the energy generated by a household that has adopted rooftop solar is $e_i = \beta\mu_L I$, where $\beta > 0$ is the scaling between mean load and net-zero size.

Let the cluster size be Q, let the fraction of households who have adopted rooftop solar be $r \in [0,1]$, and let the fraction of adopter homes that are inhabitable after the catastrophe be $\gamma \in [0,1]$. Then the reduced load of the cluster in the aftermath of the catastrophe is $L = \sum_{i=1}^{Q} fl_i$, so $L \sim \mathcal{N}(fQ\mu_L, f^2Q\sigma_L^2)$. The energy generated by the cluster is $E = \sum_{i=1}^{\gamma rQ} e_i$, so $E \sim \mathcal{N}(\gamma r\beta\mu_L Q\mu_S, \gamma^2 r^2\beta^2\mu_L^2 Q^2\sigma_S^2)$. Define $Y \equiv L - E$. We know that $Y \sim \mathcal{N}\big(Q(f\mu_L - \gamma r\beta\mu_L\mu_S), Q(f^2\sigma_L^2 + \gamma^2 r^2\beta^2\mu_L^2\sigma_S^2 Q)\big)$. Denote the mean of Y as μ_Y and the standard deviation as σ_Y.

The risk faced by the cluster is $R = P(Y > 0) = P(\frac{Y-\mu_Y}{\sigma_Y} > -\frac{\mu_Y}{\sigma_Y}) = 1 - \Phi(-\frac{\mu_Y}{\sigma_Y})$, where $\Phi(\cdot)$ is the cumulative distribution function for the standard normal distribution. The risk R is increasing in $\frac{\mu_Y}{\sigma_Y}$:

$$\frac{\mu_Y}{\sigma_Y} = \frac{Q\mu_L(f - \gamma r\beta\mu_S)}{\sqrt{Q(f^2\sigma_L^2 + \gamma^2 r^2\beta^2\mu_L^2\sigma_S^2 Q)}} = \frac{\mu_L(f - \gamma r\beta\mu_S)}{\sqrt{\frac{f^2\sigma_L^2}{Q} + \gamma^2 r^2\beta^2\mu_L^2\sigma_S^2}}. \tag{3}$$

The effect on risk of increasing the cluster size Q depends on the sign of $f - \gamma r\beta\mu_S$, which captures the balance between load and generation in the aftermath of the catastrophe. If the generation is likely to be enough, i.e. if $f - \gamma r\beta\mu_S < 0$, then R is decreasing in Q, so risk decreases with increasing cluster size. On the other hand, if the generation is unlikely to be enough, i.e. if $f - \gamma r\beta\mu_S > 0$, then risk is increasing in cluster size. The magnitude of the impact on R of changes in Q is governed by the ratio of $f^2\sigma_L^2$ to $\gamma^2 r^2\beta^2\mu_L^2\sigma_S^2$. Also, increasing cluster size leads to a limiting behavior in R:

$$\lim_{Q\to\infty} R = 1 - \Phi\bigg(-\frac{\mu_L(f - \gamma r\beta\mu_S)}{\gamma r\beta\mu_L\sigma_S}\bigg). \tag{4}$$

Thus, beyond a certain point, increasing the cluster size won't have much impact on risk.

2.4 Creating resilience clusters

Homes are grouped together into resilience clusters, each containing about the same number of homes.[2] The clustering is accomplished using a same-sized k-means algorithm using Euclidean distance based on location coordinates available for each home [24, 25]. The k-means method has deficiencies - some clusters are intermingled, some include homes that are far from each other, and the outcome varies based on the random initialization. Simple Euclidean distance does not take into account access through usable pathways. Furthermore, in a real world setting, the resilience communities that households and city planners form will be of varying sizes, will change over time, and will not be isolated from each other, particularly in the aftermath of a disaster. For the specific purpose of quantifying the effect of cluster size, however, we consider static clusters of the same size. This clustering method yields mostly reasonable clusters that are a good starting point for our analysis.

2.5 Variations studied

We compute the empirically estimated risk metric for the resilience clusters under different scenarios for adoption and cluster size. An adoption scenario A is a combination of adoption rate and adoption

[2]Specifically, the largest cluster has at most one more home in it than the smallest cluster.

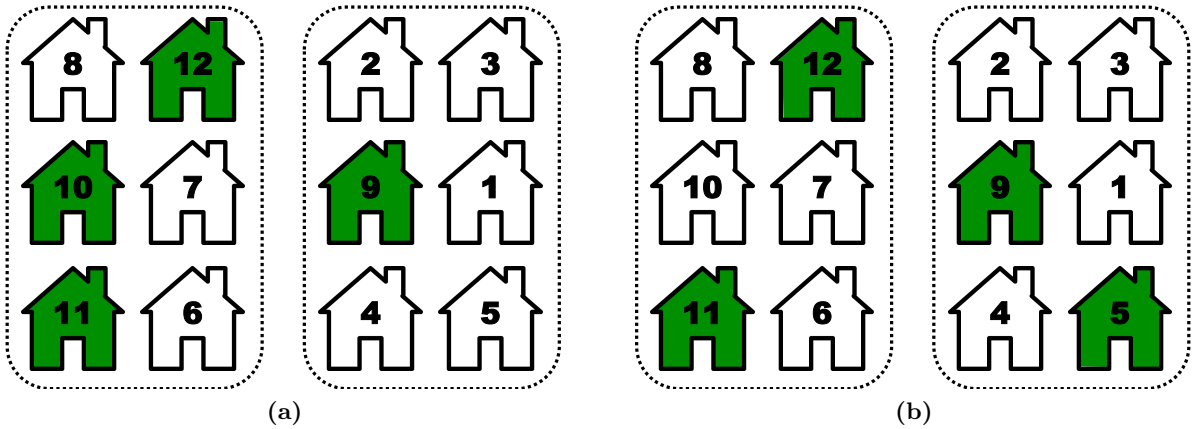

Figure 1: This figure provides an example illustrating the difference between the adoption rules. There are 12 total homes grouped into two resilience clusters of 6 homes each, with the dotted lines demarcating the clusters. The number on each house is its economic benefit b_i. The adoption rate $r = \frac{1}{3}$, and the adopters are the houses filled with green. The overall adoption rule results in the situation shown in (a), and the even adoption rule results in that shown in (b).

rule. The adoption rate r is simply the fraction of homes that have adopted rooftop solar. With N homes, the total number of adopters will be rN. The adoption rule determines *which* rN homes out of the N homes will be the adopters. We consider two different rules: overall adoption and even adoption.

First, for each home, define b_i as how much it would save on its annual electricity bill if it had a net-zero rooftop solar system. Under the overall adoption rule, the adopters are the rN homes with the highest values of b_i. By contrast, under the even adoption rule, the adopters are the homes in each cluster that are in the top r within their cluster as ordered by b_i. The even adoption rule spreads adoption out among the clusters, with the homes that stand to benefit the most within each cluster being the adopters, whereas the overall adoption rule may lead to some clusters having many more adopters than other clusters. Figure 1 illustrates the difference between the two adoption rules. The adoption pattern generated by the overall adoption rule is more in line with what households might do if left to their own devices. Those who stand to benefit more have a greater incentive to adopt rooftop solar. Achieving the adoption pattern generated by the even adoption rule would require a policy intervention.

We compute the risk under different cluster sizes in order to study the advantage of larger resilience clusters. For each cluster size, we compute one set of cluster assignments. Note that the clusters thus generated are not necessarily hierarchically nested. In other words, the clusters of size 10 are not formed by merging two clusters from the size 5 clustering results. We also note that practically speaking, the size of a resilience cluster may be limited by the logistics involved in planning and coordination among households.

We consider two values of the energy reduction fraction f: $\frac{1}{2}$ and $\frac{1}{3}$. An analysis of data from the Pecan Street Project found that for many homes, refrigeration and air conditioning made up less than 50% of total usage [26]. Communication loads (e.g. charging cell phones) are very small, as are nighttime lighting loads if LEDs are used. On this basis, we regard a reduction to $\frac{1}{2}$ as readily attainable in the aftermath of a disaster, and a reduction to $\frac{1}{3}$ as achievable with some thought.

3 Data

3.1 Building construction

The San Mateo County Tax Assessor's data provides the latitude and longitude coordinates for over 8700 single family homes in San Carlos. The data also includes the height of the home and the square footage. Figure 2 geographically depicts the homes. This data is almost complete in its coverage of single family homes in San Carlos. While the building height is available for all buildings, the number of stories is available for only 65% of the buildings. We performed a Bayesian inference based on the building height to estimate the most likely number of stories for the buildings without this information, using a cutoff height of 14 feet to separate single story homes from two story homes.

3.2 Electrical energy consumption

The household electrical energy consumption data comes from smart meters for over 1800 single family homes in San Carlos and 46 single family homes in nearby Redwood City, California. The smart meters recorded hourly electrical energy consumption for each home from November 1, 2011, to October 31, 2012. We exclude any meters with less than 0.1 kW annual mean consumption or with more than half of the readings being zero. We sum the hourly data each day to produce the daily electrical energy consumption for each home, $\tilde{l}_{i,d}$. Figure 3 characterizes the energy consumption data by giving the distributions of various load statistics for each household.

We have survey data that includes the year built and a square footage range for each home. Figure 4 shows the relationship between average daily consumption and these home characteristics. The Redwood City smart meters are included to augment the small number of San Carlos meters available in the 501-750, 4001-5000, and 5001-10000 square foot ranges. There is a definite relationship between the area of a home and its energy consumption, while there is no evidence of a relationship between consumption and year built.

3.3 Combining energy and construction data

The energy consumption data does not contain precise location information for the meters. In addition, we only have energy consumption data for 1900 homes, while there are 8700 homes in the construction data. Therefore we cannot perform a precise one-to-one matching between the consumption data and the construction data. As shown in Figure 4b, square footage is correlated with electrical energy consumption. This relationship motivates the use of stratified sampling based on square footage in order to assign meter data to buildings, as described in Algorithm 1.

3.4 Solar energy generation and economic benefit

We follow [27] for defining the solar irradiance and net-zero system sizes for each home.[3] Together, these produce $\tilde{e}_{i,d}$, the energy that each household would generate if it had a net-zero rooftop solar system. We use the annual bill savings computed in that study as the economic benefit b_i, assuming that households purchase electricity at the retail time of use rate and sell any surplus back at the

[3]The homes in San Carlos are in one zip code, so they all experience the same irradiance.

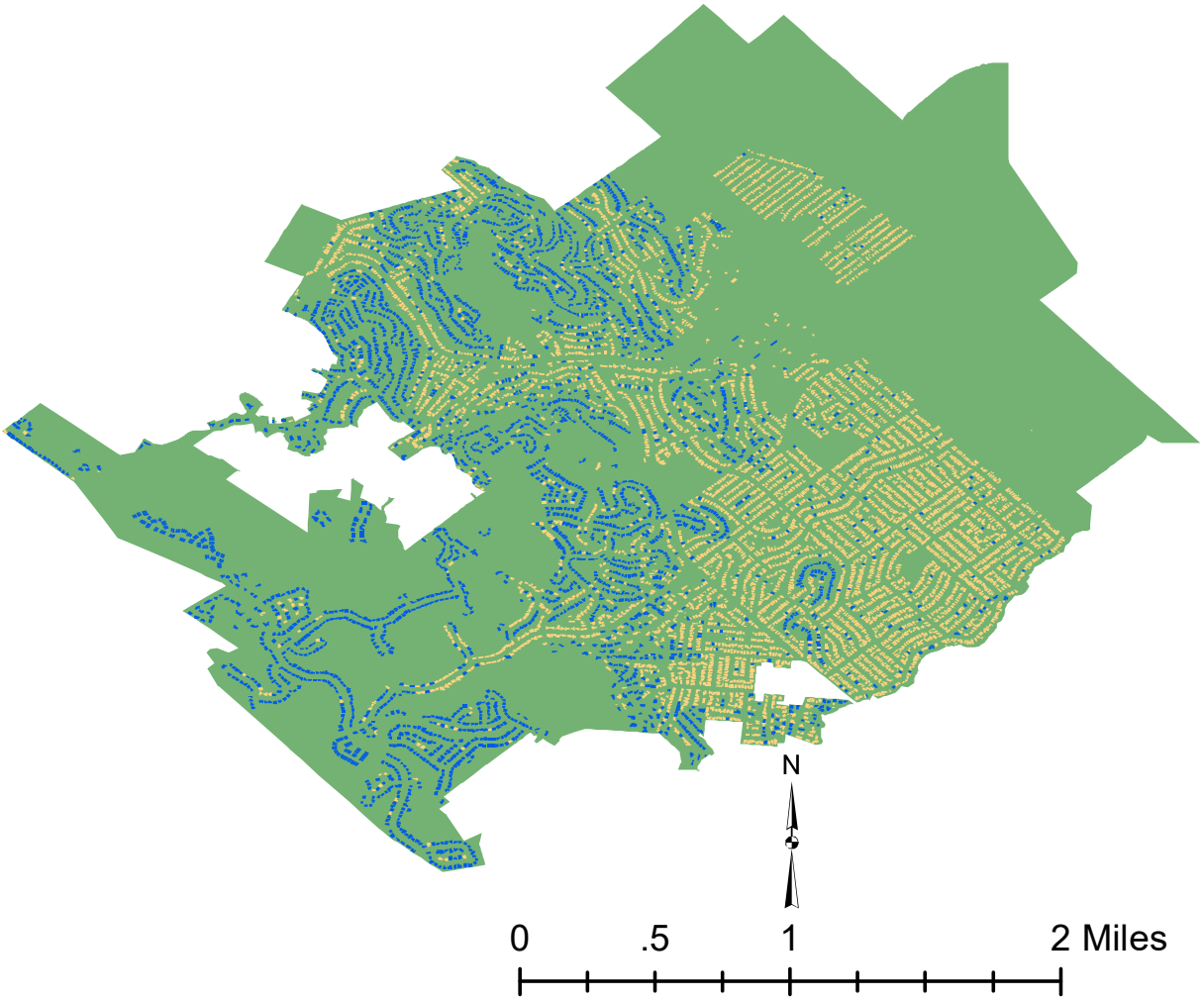

Figure 2: The building construction data comes from the tax assessor's file. Single family homes with a height less than or equal to 14 feet are light orange, and those with a height greater than 14 feet are blue. That cutoff is related to an assumption about one story versus two story homes that is used in the earthquake damage modeling. The green shaded area marks the extent of the city of San Carlos.

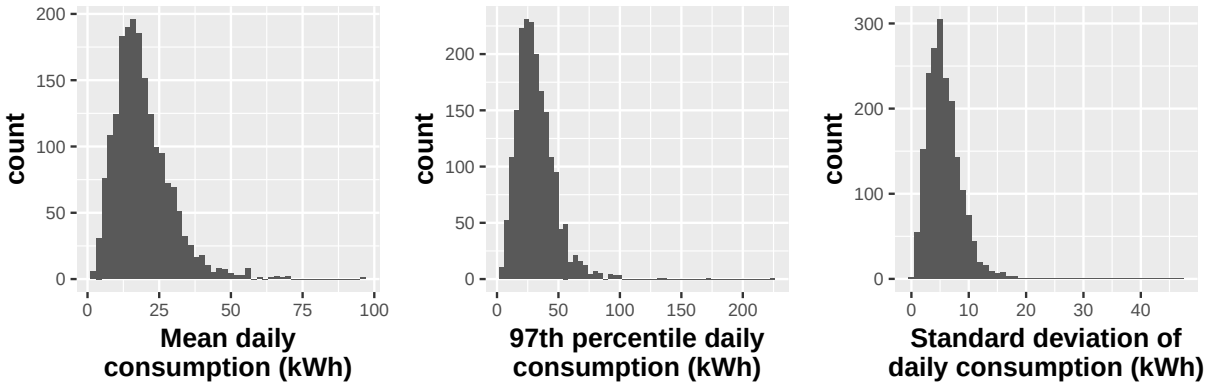

(a) (b) (c)

Figure 3: These figures provide distributions of statistics of the daily load for each household. The statistics are computed over a year's worth of data for each household.

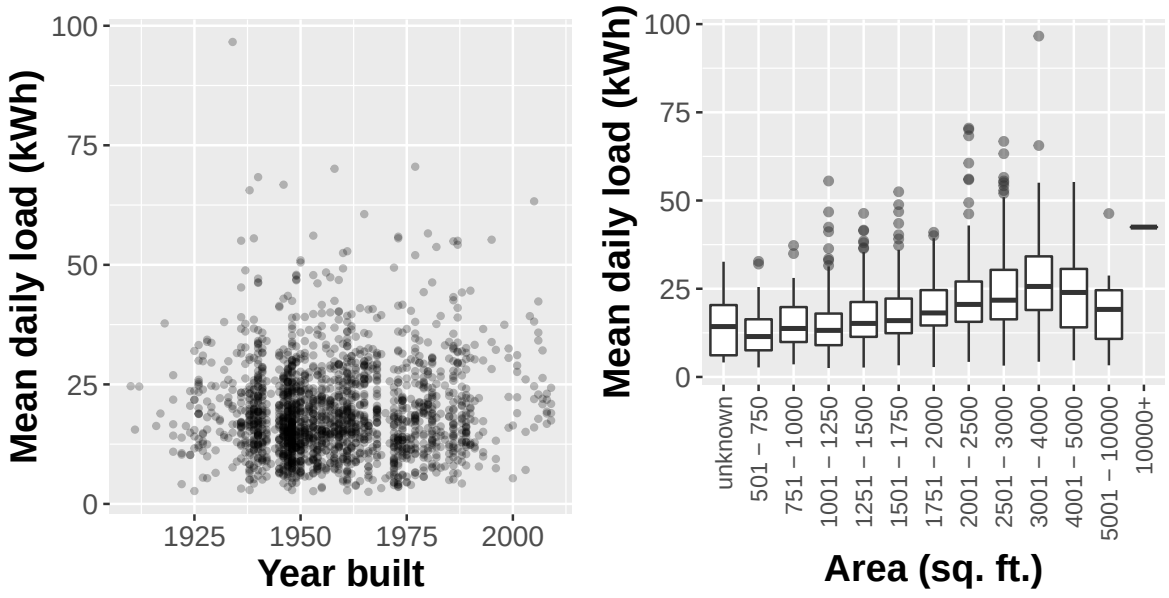

(a) (b)

Figure 4: These figures capture the relationship between mean daily load and characteristics of the home in the energy consumption data. (a) There is not a strong relationship between mean daily load and year built. (b) Mean daily load generally increases with the square footage of the home. Note that there are only ten meters from homes in the $5001 - 10000$ square feet range, and only one in the 10000+ range, so that information is less reliable.

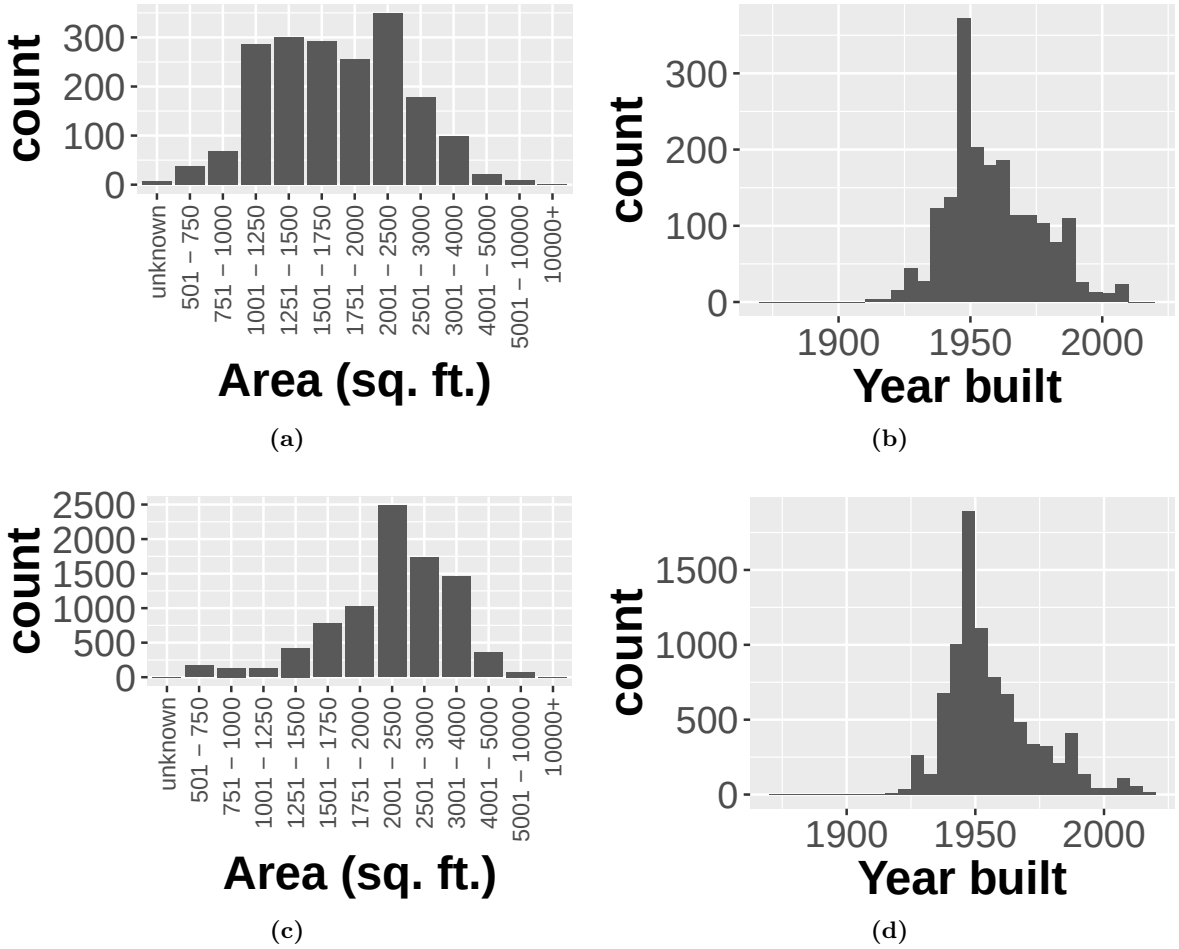

Figure 5: The area and year built of homes in the energy consumption data are shown in (a) and (b), while (c) and (d) show the same for the homes in the building construction data. As a population, the homes in the energy consumption data are smaller and somewhat newer than the homes in the construction data, which is more representative of the stock of single family homes in San Carlos. One possible explanation for this bias is that the survey responses for the energy consumption data are self-reported, and people are more likely to decline to state large home sizes, whereas the building construction data is gathered directly by a public official.

Algorithm 1 Stratified sampling procedure for assigning smart meter data to homes in construction data. The inputs to this algorithm are as follows: a partition of possible home areas $A = \{A_1, \ldots, A_P\}$ corresponding to the ranges used in the consumption data survey information (e.g. the numerical ranges on the x-axis of Figure 4b); the set of meter readings $U = \{U_1, \ldots, U_R\}$; for each meter reading U_j, $\tilde{a}_j$ is the element of the area partition reported in the survey information; the set of homes $H = \{H_1, \ldots, H_N\}$ from the construction data; the area a_i of each home H_i.

for k =1,P **do**
  $U^k \leftarrow \{U_j \mid \tilde{a}_j = A_k\}$ ▷ U^k is all meters whose survey data shows area range A_k
  $B^k \leftarrow U^k$
for i=1,N **do**
  Find k such that $a_i \in A_k$ ▷ Find the area range for home H_i
  if B^k is empty **then**
    $B^k \leftarrow U^k$
  Choose b uniformly at random from B^k
  $l_i \leftarrow b$ ▷ H_i's load l_i comes from a home with same area range
  $B^k \leftarrow B^k \setminus b$ ▷ Sample without replacement and refill when needed

wholesale rate.[4] The annual bill savings for a household are strongly positively correlated with its net-zero system size.

3.5 Earthquake simulations

The catastrophe C in our study is modeled after the 1906 San Francisco earthquake in terms of the magnitude and the fault. The geometry of the 1906 rupture was extracted from the Uniform California Earthquake Rupture Forecast (UCERF) version 2 through the OpenSHA engine [28, 29]. Average spectral accelerations, Sa_{av}, were computed in San Carlos to represent the shaking intensity measure. Sa_{av} is defined as the geometric mean of the spectral accelerations, Sa, between 0.2 and 3 times a fundamental period of vibration. We choose a period of 0.16 seconds because [30] demonstrates that it best correlates with seismic damage in 1- and 2-story wooden buildings, which together represent more that 99.5% of the building typologies in our case study. We computed 500 realizations of spatially distributed Sa_{av} using the ground motion model in [31], incorporating a spatial correlation structure from [32]. The set $\tilde{C}$ contains the 500 realizations as its elements. We assume that every realization causes a power outage span of one day, so $s(\tilde{c}) = 1$ for all $\tilde{c}$.[5]

In a post-earthquake setting, buildings are red tagged by trained engineers if the buildings are unsafe to be occupied. We simulate the post-earthquake building tagging by using fragility functions developed for 1- and 2-story wooden single-family residential buildings [30]. These functions evaluate the likelihood that a building is red tagged after an earthquake as a function of Sa_{av}. Using these data and models, the probability of being red tagged $p_i(\tilde{c})$ is calculated for each home i and for each earthquake realization $\tilde{c}$. Then, this probability is used to sample from a Bernoulli

[4] In [27], homes adopt a net-zero sized PV system as well as a storage device scaled to the size of the PV system. The storage device itself is responsible for a small fraction of a household's total bill savings.

[5] More detailed analysis could give better estimates of the earthquake power outage timespan. Our assumption was based on previous medium- and large-magnitude earthquake observations that left thousands of households without power for several days (e.g., 1989 Loma Prieta, 1994 Northridge, and the 2014 Napa earthquakes). Note that longer outage spans will lead to higher values of risk, all else being equal.

distribution to determine whether the home will be red tagged or not. We deem that red tagged homes are uninhabitable, and thus if home i is red tagged, we set $x_i(\tilde{c}) = 1$.[6] In other words, $x_i(\tilde{c}) \sim \text{Bernoulli}(p_i(\tilde{c}))$. Figure 6 shows the proportion of times that a given home is deemed uninhabitable across all 500 realizations of the earthquake.

4 Results

The energy resilience in this study is provided entirely by rooftop solar, so the risk metrics are strongly seasonal. We estimate the risk for T being the whole year for which we have consumption data, as well as for T being each season within that year. As shown in Figure 7, the median cluster risk can vary from close to zero in summer all the way to one in winter. Even with an adoption rate of 100% and a reduction fraction of $f = \frac{1}{3}$, the median risk in winter remains at 0.4 for all cluster sizes. Thus, either a different generation technology or a different approach to system sizing would be required to provide high levels of resilience to outages during winter. From here on, we will focus on metrics for either the entire year or for seasons other than winter.

4.1 Increasing adoption

Figure 8 illustrates the effect of increasing adoption of rooftop solar on reducing risk. Increasing adoption steadily shifts the distribution of whole-year cluster risk downward. For the summer season, however, the risk is almost entirely eliminated at about 20-25% adoption. Thus, one home with a net-zero panel is very likely to be able to support the energy needs of three or four neighbors during an outage in summer if they can all manage to cut their consumption to $\frac{1}{3}$ of their usual usage.

As seen in Figure 8c, a small decrease in adoption from 15% to 10% can lead to a large and widespread increase in risk. The same results are depicted geographically in 10c as compared with 10a. This sensitivity point is a function of how much energy a home with a net-zero system will generate in excess of its own needs. In this particular case, one home with a net-zero system can reliably support the reduced energy needs of about 7 homes but no more. The decrease from three adopters in a cluster of 20 to just two makes a big difference.

4.2 Different adoption rules

By design, the even adoption rule leads to much more even risk across clusters. As shown in Figure 8c vs. 8d, the median cluster risk is similar for both adoption rules, but the dispersion is much wider under overall adoption. This same effect is evident when comparing Figures 10a and 10b, showing many more homes belonging to clusters with high risk in the overall adoption case.

The total system size adopted, and the total bill savings of the adopters, will vary under the overall and even adoption rules. For the cases in the figures just mentioned, the cluster size is 20 and the adoption rate is 15%. Under the overall adoption rule, the total system size adopted is 12.4 MW, and the total annual bill savings is $3.02 million. Under the even adoption rule, the total system size adopted is 11.8 MW, and the total annual bill savings is $2.87 million.

[6] Note that in an actual earthquake, it may take some time for an engineer to show up and officially red tag a building. We assume, however, that the occupants would abandon such a home out of caution right after the earthquake.

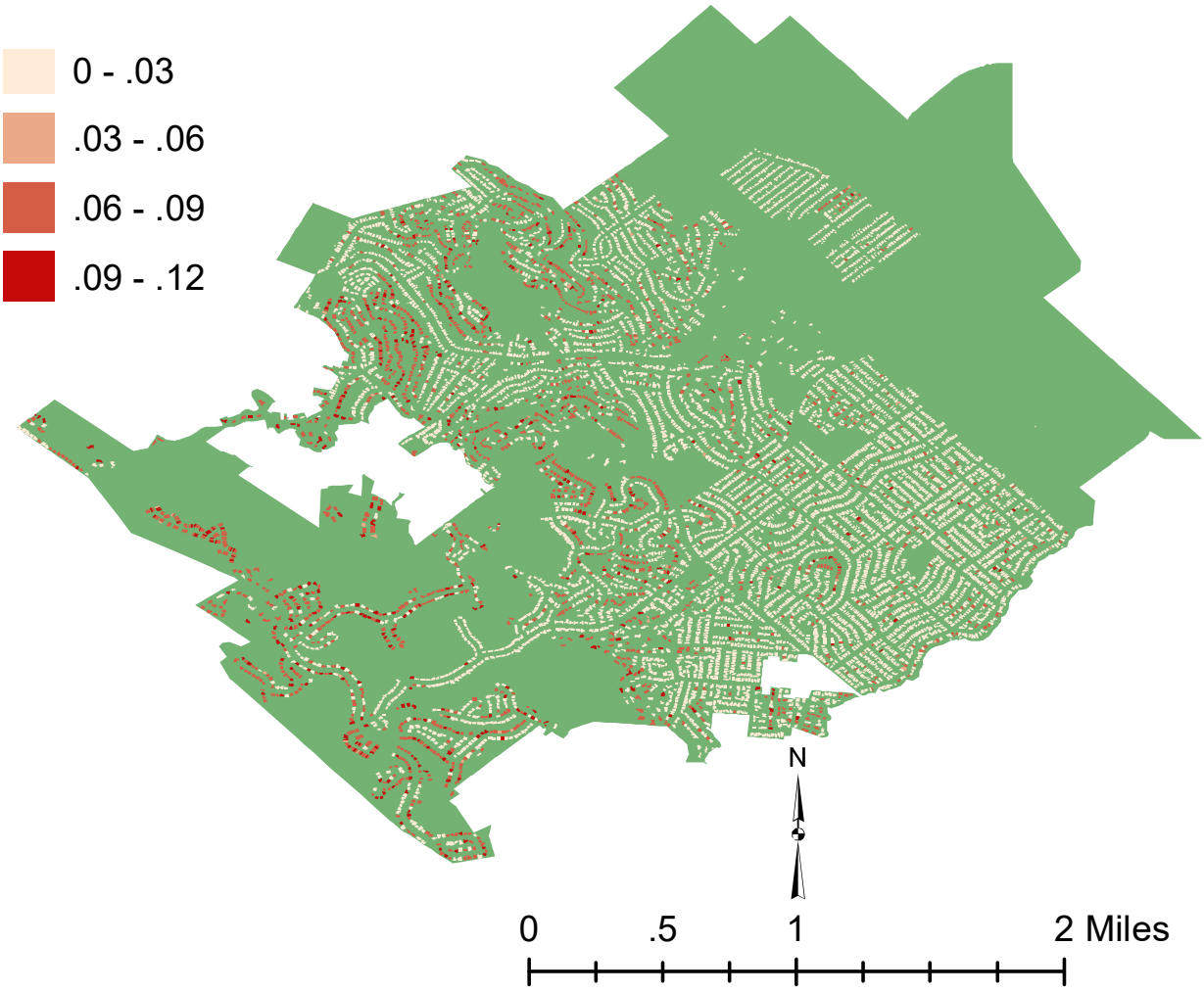

Figure 6: This figure depicts the proportion of times that a home is deemed uninhabitable across the 500 simulations of the 1906 San Francisco earthquake. The distribution is bimodal, with two story homes more likely to be red-tagged than one story homes, as can be seen by comparing this figure to Figure 2.

4.3 Increasing cluster size

Figure 9 illustrates the effect of increasing cluster size for a fixed adoption rate and reduction fraction f. The effect of cluster size varies depending on the adoption rule. The even adoption rule satisfies some of the conditions of the theoretical model presented in Section 2.3. For the case depicted in Figure 9a, the fundamental balance between generation and load in the aftermath of the earthquake tilts in favor of generation, so increasing cluster size reduces risk as in the theoretical model. The model's limiting behavior of risk with respect to increasing cluster size is also apparent in the figure, with most of the benefit achieved at a cluster size of 20-25.

The homes in our study, however, have heterogeneous loads, which is a departure from the theoretical model. As a consequence, with even adoption, the adopting households will be different for different cluster sizes. At larger cluster sizes, it becomes more and more the case that the households who save the most overall — and therefore have the largest net-zero system size — are the adopters.[7] This increases the total adopted system size, which has a direct impact on reducing the risk. For example, in Figure 9a, the total adopted system size is 14.1 MW for cluster size 5, 15.0 MW for cluster size 30, and 15.1 MW for cluster size 50. The total adopted system size with overall adoption is 15.3 MW.

By contrast, under the overall adoption rule, the adopting households are the same for different cluster sizes, so the total adopted system size is the same. Thus, the improvement in risk seen in Figure 9b, in particular the shift downward at the upper end of the distribution, is due to improved sharing with larger groups. Specifically, as the cluster size increases, it becomes less and less likely that any given cluster will have no adopters in it. Thus, the worst case cluster risk decreases. There is no clear trend for the median risk.

5 Discussion

We present a methodology for conducting a first order assessment of the contribution of distributed energy resources to energy resilience in the aftermath of a catastrophe. Resilience officers can apply our methods to estimate how increasing rooftop solar adoption will affect risk related to outages in their neighborhoods. This type of assessment lays the groundwork for developing metrics that account for the resilience value of rooftop solar in addition to its value in terms of bill savings and sustainability. In addition, quantifying the benefits of clustering and sharing can help inform resilience planning efforts in residential communities. We find that increasing the size of a resilience cluster can be beneficial or detrimental depending on the fundamental statistics of energy balance within a cluster in the aftermath of the disaster.

Turning to the adoption rule comparison, if households that stand to save the most from rooftop solar adopt first, the resulting adoption pattern will be close to that of the overall adoption rule. In our study, we find that overall adoption can lead to large and widespread disparities in risk, with some clusters at much lower risk than others. Bill savings are higher for homes with larger net-zero systems, which are homes that consume more energy. These also tend to be larger homes. We find a negative correlation between home square footage and risk for the case depicted in Figure 10b, despite the fact that larger homes are more often red tagged after the earthquake because they are more likely to have two stories. In other words, neighborhoods with larger homes sustain more

[7] In the limit, with a single cluster containing all households, the even adoption rule results in the same adopters as the overall adoption rule.

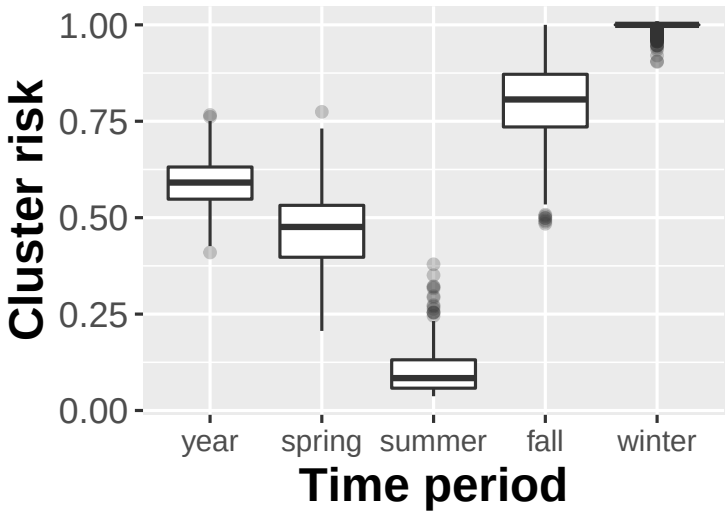

Figure 7: The cluster risk is strongly seasonal because the resilience clusters rely on solar energy to meet their needs. Note in particular the dramatic difference between summer, where the median cluster risk is around 0.1, and winter, where the median risk is at its maximum possible level of 1. For this figure, the cluster size is 20, the adoption level is 15%, the adoption rule is even adoption, and the reduction fraction $f = \frac{1}{3}$.

loss of rooftop PV generation but are nonetheless more likely to be able to meet their electrical energy needs. These neighborhoods tend to be inhabited by people with more wealth and income, so disparities in risk overlap with economic disparities.

Policymakers interested in evening out risk could seek to encourage adoption patterns closer to those generated by the even adoption rule. For the case shown in Figure 10a, which is the same as Figure 10b but with even adoption, there is a small but *positive* correlation between home square footage and risk. The neighborhoods with larger homes are now *less* likely to meet their energy needs due to the greater loss of PV that they suffer. We can compare the overall and even adoption rules economically based on the total adopted system size and the total bill savings for the two cases as reported in Section 4.2. Suppose that, under either rule, the adopters as a group attempt to fund their purchase of the rooftop solar systems out of their bill savings. Their per unit bill savings is the key figure that they would compare to the per unit costs of rooftop solar systems. Because the total number of adopters is the same in both cases, we assume that the fixed costs are the same. In the overall adoption case, the annual bill savings divided by the system size comes to \$244.2/year/kW; in the even adoption case, that figure is just slightly lower at \$242.8/year/kW. If a policymaker augmented the total bill savings of the adopters under even adoption by \$16,700/year, then their per unit bill savings would match that of the adopters under overall adoption. The policymaker would need to compare that annual augmentation with costs of other methods to reduce risk.

Our study poses even adoption and overall adoption as exclusive alternatives in order to cleanly compare them. In order to perfectly implement the even adoption rule, however, the policymaker would have to prohibit additional adoption in clusters that already had the right number of adopters. Thus, some clusters would face higher risk under even adoption than they would under overall adoption. This is not feasible or desirable from the standpoint of promoting the adoption of distributed energy resources. Any real policy intervention aimed at more evenly dispersed adoption

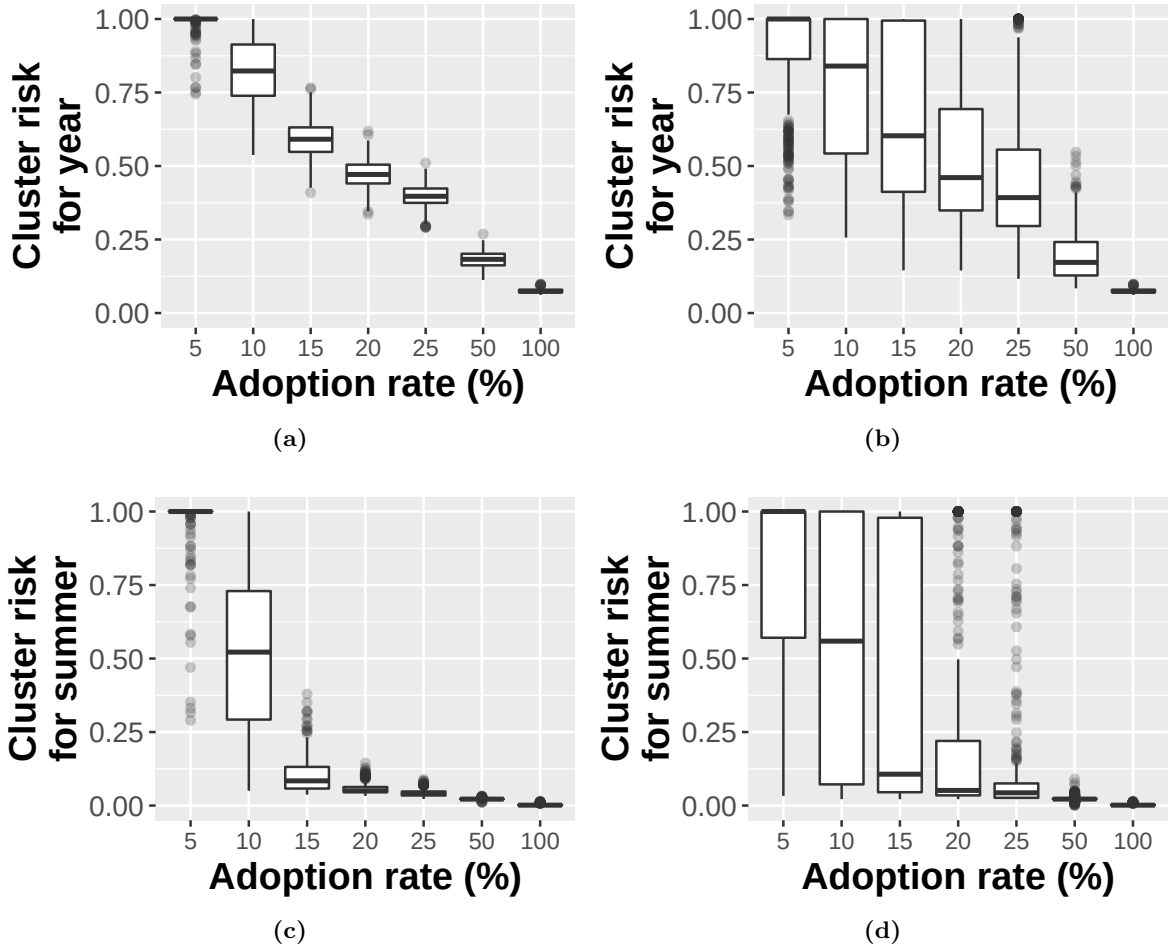

Figure 8: The cluster risk for cluster size 20 and $f = \frac{1}{3}$ is shown as a function of the adoption rate. The left two panels are for the even adoption rule, the right two for the overall adoption rule. Note that the increase in adoption from 5-25% is in linear steps, whereas the last two steps to 50% and 100% represent a geometric increase.

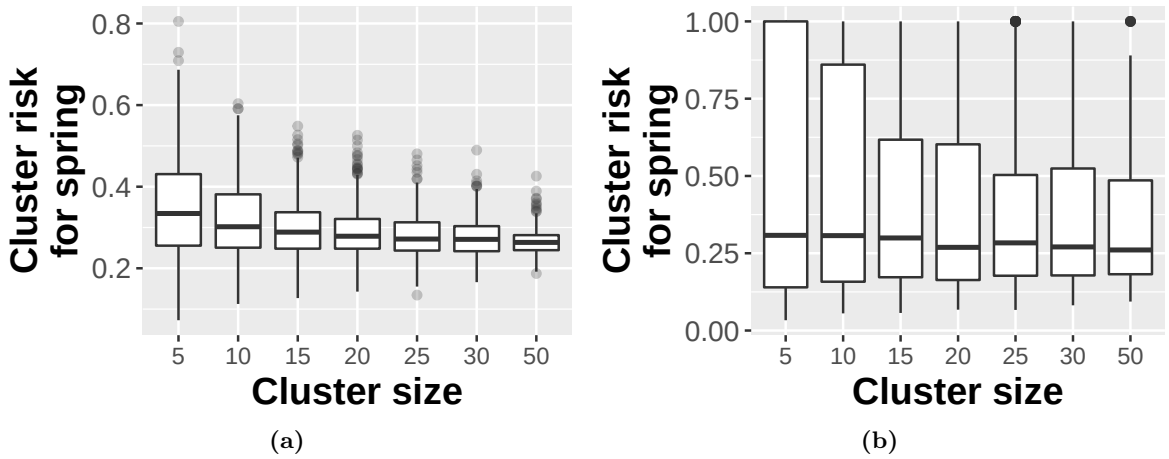

Figure 9: The cluster risk for spring with $f = \frac{1}{3}$ and an adoption rate of 20% is shown as a function of cluster size for the (a) even adoption rule and (b) overall adoption rule. Note that the last step from size 30 to 50 is much larger than prior steps.

is likely to result in an adoption scenario somewhere between even and overall adoption. Some clusters, those with larger homes and greater potential bill savings, will end up with a greater fraction of adopters, and other clusters will require targeted help to achieve some minimum level of adoption for resilience.

We identify three key steps to advance this study. The first is to translate our risk metrics into dollar terms. There are direct costs to disaster related outages, like spoiled food and medicine, productivity loss, and damage to home equipment. Some of these can be mitigated by reducing outage risk as proposed in our study. More importantly, making neighborhoods more resilient makes it more likely that people will stay in their communities in the aftermath of a disaster, avoiding the direct costs and economic dislocation of evacuation, resettlement, and return. Quantifying these avoided costs may be more important than the direct costs of outages in residential communities. The second extension is to address the distribution of energy — how to physically share energy between homes, and how to deal with the mismatch in timing between generation and consumption through storage and other means. Finally, we note that electrical energy resilience is only one part of what makes a residential community livable in the aftermath of a disaster. Water and communication infrastructure are also essential. A holistic framework that accounts for the interactions of these and other systems would be an important contribution to modeling and quantifying resilience.

Acknowledgements

We thank Pacific Gas and Electric Company for providing the smart meter data used in this study. We thank Irene Alisjahbana for reviewing studies of earthquake damage to power systems and recent developments in microgrids. We thank Emily Alcazar for laying the groundwork for the geographic risk visualizations.

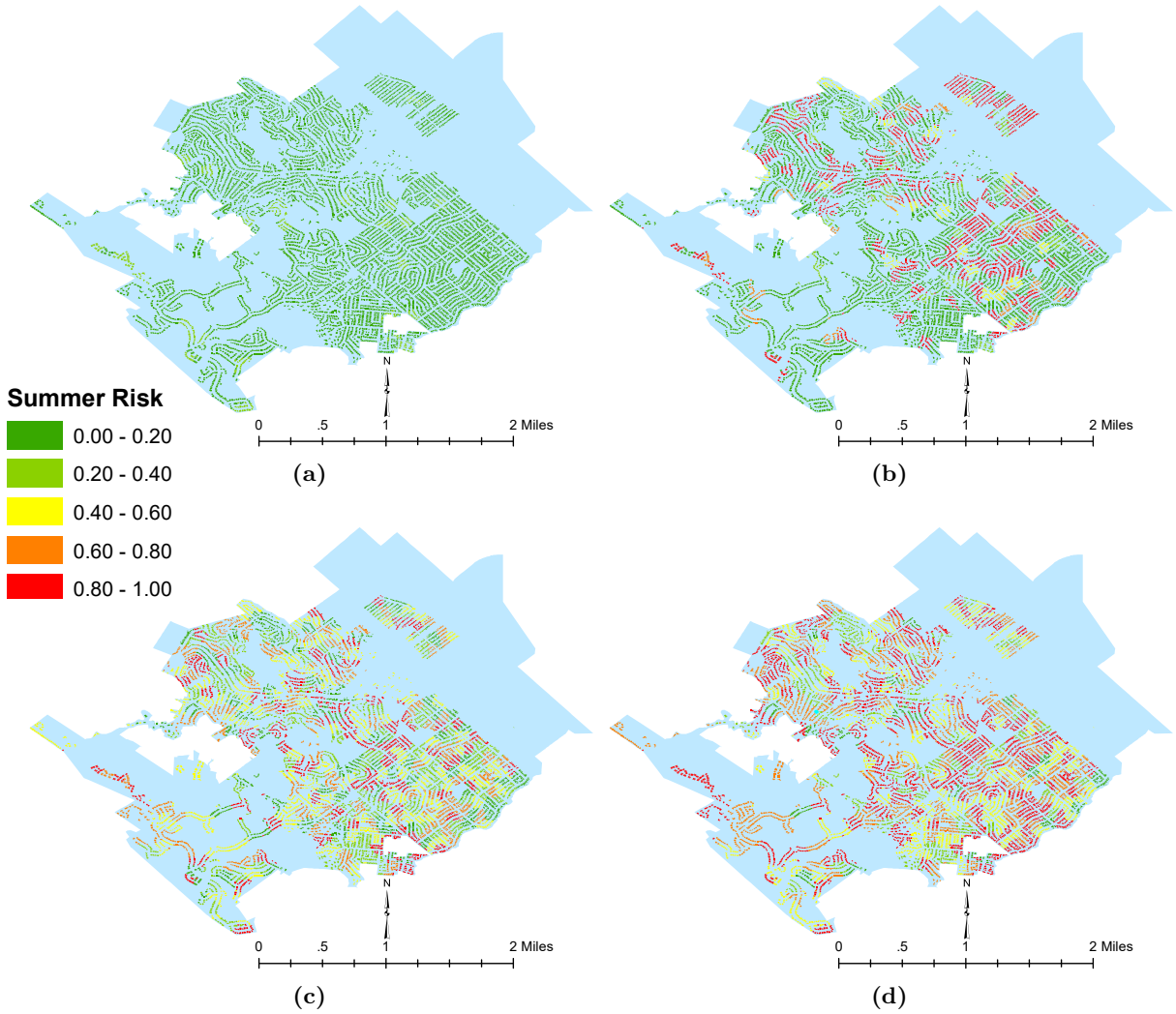

Figure 10: These images geographically depict the risk faced by the households during summer under varying conditions. Each home is colored based on the risk value for the cluster to which it belongs. (a) The homes face relatively low risk when they are grouped into resilience clusters of size 20, with rooftop solar adoption rate of 15% with the even adoption rule, and with reduction fraction $f = \frac{1}{3}$. (b) The conditions are the same as in (a) but with the adoption rule changed to overall adoption. Now the risk is much more uneven across the homes, as would be expected. The overall adoption rule can lead to very uneven adoption among clusters, with some clusters having no homes with rooftop solar. (c) The conditions are the same as in (a) but with the adoption rate reduced to 10%. This decreases the number of adopters in a typical cluster from three to two, dramatically driving up the risk for many homes. (d) The conditions are the same as in (a) but with $f = \frac{1}{2}$. Consistently meeting this higher fraction of the original load is much harder with net-zero sized rooftop solar, leading to higher risk across the city.

References

[1] F. H. Norris, S. P. Stevens, B. Pfefferbaum, K. F. Wyche, and R. L. Pfefferbaum, "Community resilience as a metaphor, theory, set of capacities, and strategy for disaster readiness," *American Journal of Community Psychology*, vol. 41, no. 1-2, pp. 127–150, 2008.

[2] S. L. Cutter, L. Barnes, M. Berry, C. Burton, E. Evans, E. Tate, and J. Webb, "A place-based model for understanding community resilience to natural disasters," *Global Environmental Change*, vol. 18, no. 4, pp. 598 – 606, 2008.

[3] M. Bruneau, S. E. Chang, R. T. Eguchi, G. C. Lee, T. D. ORourke, A. M. Reinhorn, M. Shinozuka, K. Tierney, W. A. Wallace, and D. von Winterfeldt, "A Framework to Quantitatively Assess and Enhance the Seismic Resilience of Communities," *Earthquake Spectra*, vol. 19, no. 4, pp. 733–752, 2003.

[4] D. R. Godschalk, "Urban hazard mitigation: creating resilient cities," *Natural Hazards Review*, vol. 4, no. 3, pp. 136–143, 2003.

[5] D. Mitsova, A.-M. Esnard, A. Sapat, and B. S. Lai, "Socioeconomic vulnerability and electric power restoration timelines in Florida: the case of Hurricane Irma," *Natural Hazards*, Aug 2018.

[6] M. Gallucci, "Rebuilding Puerto Rico's Grid," *IEEE Spectrum*, vol. 55, no. 5, pp. 30–38, May 2018.

[7] J. C. Araneda, H. Rudnick, S. Mocarquer, and P. Miquel, "Lessons from the 2010 Chilean earthquake and its impact on electricity supply," in *Power System Technology (POWERCON), 2010 International Conference on.* IEEE, 2010, pp. 1–7.

[8] A. Kwasinski, J. Eidinger, A. Tang, and C. Tudo-Bornarel, "Performance of Electric Power Systems in the 2010-2011 Christchurch, New Zealand, Earthquake Sequence," *Earthquake Spectra*, vol. 30, no. 1, pp. 205–230, 2014.

[9] R. Liu, M. Zhang, and Y. Wu, "Vulnerability Study of Electric Power Grid in Different Intensity Area in Wenchuan Earthquake," in *15th World Conference of Earthquake Engineering (WCEE), Lisboa, Portugal*, 2012.

[10] L. Johnson and S. Mahin, "The Mw 6.0 South Napa Earthquake of August 24, 2016," California Seismic Safety Commission, Sacramento, CA, Tech. Rep., 2016. [Online]. Available: http://www.seismic.ca.gov/minutes/04B-NapaEQLessonsLearned{_}WorkingDraft-FindingsOnly{_}010716.pdf

[11] Z. Wang and J. Wang, "Self-Healing Resilient Distribution Systems Based on Sectionalization Into Microgrids," *IEEE Transactions on Power Systems*, vol. 30, no. 6, pp. 3139–3149, Nov 2015.

[12] A. Gholami, F. Aminifar, and M. Shahidehpour, "Front Lines Against the Darkness: Enhancing the Resilience of the Electricity Grid Through Microgrid Facilities," *IEEE Electrification Magazine*, vol. 4, no. 1, pp. 18–24, March 2016.

[13] C. Chen, J. Wang, F. Qiu, and D. Zhao, "Resilient Distribution System by Microgrids Formation After Natural Disasters," *IEEE Transactions on Smart Grid*, vol. 7, no. 2, pp. 958–966, March 2016.

[14] P. Basak, S. Chowdhury, S. H. nee Dey, and S. Chowdhury, "A literature review on integration of distributed energy resources in the perspective of control, protection and stability of microgrid," *Renewable and Sustainable Energy Reviews*, vol. 16, no. 8, pp. 5545 – 5556, 2012.

[15] W. I. Bower, D. T. Ton, R. Guttromson, S. F. Glover, J. E. Stamp, D. Bhatnagar, and J. Reilly, "The Advanced Microgrid: Integration and Interoperability," Sandia National Laboratories, Albuquerque, NM (United States), Tech. Rep., 2014.

[16] M. Hyams, A. Awai, T. Bourgeois, K. Cataldo, and S. Hammer, "Microgrids: an assessment of the value, opportunities and barriers to deployment in new york state," *New York State Energy Research and Development Authority*, 2011.

[17] M. T. Burr, M. J. Zimmer, B. Meloy, J. Bertrand, W. Levesque, G. Warner, and J. D. McDonald, *Minnesota microgrids: barriers, opportunities, and pathways toward energy assurance*. Minnesota Department of Commerce, 2013.

[18] C. Villarreal, D. Erickson, and M. Zafar, "Microgrids: A Regulatory Perspective," *California Public Utilities Commission*, 2014.

[19] S. Lahiri, B. Olof, F. Richard, T. Nellie, and G. DNV, "Microgrid Assessment and Recommendation(s) to Guide Future Investments," *California Energy Commission, Publication Number CEC-500–2015–071*, 2015.

[20] C. Marnay, H. Aki, K. Hirose, A. Kwasinski, S. Ogura, and T. Shinji, "Japan's pivot to resilience: How two microgrids fared after the 2011 earthquake," *IEEE Power and Energy Magazine*, vol. 13, no. 3, pp. 44–57, 2015.

[21] California Energy Commission *et al.*, "New Residential Zero Net-Energy Action Plan 2015-2020," *CA Energy Efficiency Strategic Plan*, 2015.

[22] California Energy Commission. (2018) Energy Commission Adopts Standards Requiring Solar Systems for New Homes, First in Nation. [Online]. Available: http://www.energy.ca.gov/releases/2018_releases/2018-05-09_building_standards_adopted_nr.html

[23] V. Fthenakis, "The resilience of PV during natural disasters: The hurricane Sandy case," in *2013 IEEE 39th Photovoltaic Specialists Conference (PVSC)*, June 2013, pp. 2364–2367.

[24] ELKI. Same-size k-Means Variation. [Online]. Available: https://elki-project.github.io/tutorial/same-size_k_means

[25] E. Schubert, A. Koos, T. Emrich, A. Züfle, K. A. Schmid, and A. Zimek, "A Framework for Clustering Uncertain Data," *Proceedings of the VLDB Endowment*, vol. 8, no. 12, pp. 1976–1979, 2015.

[26] B. Glasgo, C. Hendrickson, and I. M. Azevedo, "Using advanced metering infrastructure to characterize residential energy use," *The Electricity Journal*, vol. 30, no. 3, pp. 64 – 70, 2017.

[27] S. Patel and R. Rajagopal, "The Value of Distributed Energy Resources for Heterogeneous Residential Consumers," arXiv preprint arXiv:1709.08140, September 2018.

[28] E. H. Field, T. E. Dawson, K. R. Felzer, a. D. Frankel, V. Gupta, T. H. Jordan, T. Parsons, M. D. Petersen, R. S. Stein, R. J. Weldon, and C. J. Wills, "Uniform California earthquake rupture forecast, version 2 (UCERF 2)," *Bulletin of the Seismological Society of America*, vol. 99, no. 4, pp. 2053–2107, 2009.

[29] E. Field, T. Jordan, and C. Cornell, "A Developing Community-Modeling Environment for Seismic Hazard Analysis," *Seismological Research Letters*, vol. 74, no. 44, pp. 406–419, 2003.

[30] P. Heresi and E. Miranda, "Evaluation of intensity measures for wood-frame low-rise structures," 2018, in progress.

[31] H. Davalos and E. Miranda, "A Ground Motion Prediction Model for Average Spectral Acceleration," *Earthquake Engineering & Structural Dynamics*, 2018.

[32] P. Heresi and E. Miranda, "Fragility curves for yellow- and red-tagging of single-family houses," 2018, in progress.